Earth Syst. Sci. Data, 14, 3599–3613, 2022
https://doi.org/10.5194/essd-14-3599-2022


Open Access Earth System Science Data

# The Landscape Fire Scars Database: mapping historical burned area and fire severity in Chile

**Alejandro Miranda[1,2], Rayén Mentler[1], Ítalo Moletto-Lobos[3], Gabriela Alfaro[4], Leonardo Aliaga[1], Dana Balbontín[1], Maximiliano Barraza[1], Susanne Baumbach[1], Patricio Calderón[1], Fernando Cárdenas[1], Iván Castillo[1], Gonzalo Contreras[1], Felipe de la Barra[4], Mauricio Galleguillos[1,5], Mauro E. González[1,6,7], Carlos Hormazábal[1], Antonio Lara[1,6,8], Ian Mancilla[1], Francisca Muñoz[1], Cristian Oyarce[1], Francisca Pantoja[1], Rocío Ramírez[1], and Vicente Urrutia[1]**

[1]Center for Climate and Resilience Research, (CR)[2], Santiago, Chile
[2]Laboratorio de Ecología del Paisaje y Conservación, Departamento de Ciencias Forestales, Universidad de La Frontera, Temuco, Chile
[3]Image Processing Laboratory, Global Change Unit, University of Valencia, Valencia, Spain
[4]Industrial Engineering Department, University of Chile, Santiago, Chile
[5]Facultad de Ingeniería y Ciencias, Universidad Adolfo Ibáñez, Santiago, Chile
[6]Instituto de Conservación, Biodiversidad y Territorio, Facultad de Ciencias Forestales y Recursos Naturales, Universidad Austral de Chile, Valdivia, Chile
[7]Center for Fire and Socioecosystem Resilience (FireSES), Universidad Austral de Chile, Valdivia, Chile
[8]Fundación Centro de los Bosques Nativos FORECOS, Valdivia, Chile

**Correspondence:** Alejandro Miranda (alejandro.miranda@ufrontera.cl)

Received: 17 February 2022 – Discussion started: 29 March 2022
Revised: 4 July 2022 – Accepted: 16 July 2022 – Published: 10 August 2022

**Abstract.** Achieving a local understanding of fire regimes requires high-resolution, systematic and dynamic databases. High-quality information can help to transform evidence into decision-making in the context of rapidly changing landscapes, particularly considering that geographical and temporal patterns of fire regimes and their trends vary locally over time. Global fire scar products at low spatial resolutions are available, but high-resolution wildfire data, especially for developing countries, are still lacking. Taking advantage of the Google Earth Engine (GEE) big-data analysis platform, we developed a flexible workflow to reconstruct individual burned areas and derive fire severity estimates for all reported fires. We tested our approach for historical wildfires in Chile. The result is the Landscape Fire Scars Database, a detailed and dynamic database that reconstructs 8153 fires scars, representing 66.6 % of the country's officially recorded fires between 1985 and 2018. For each fire event, the database contains the following information: (i) the Landsat mosaic of pre- and post-fire images; (ii) the fire scar in binary format; (iii) the remotely sensed estimated fire indexes (the normalized burned ratio, NBR, and the relative delta normalized burn ratio, RdNBR); and two vector files indicating (iv) the fire scar perimeter and (v) the fire scar severity reclassification, respectively. The Landscape Fire Scars Database for Chile and GEE script (JavaScript) are publicly available. The framework developed for the database can be applied anywhere in the world, with the only requirement being its adaptation to local factors such as data availability, fire regimes, land cover or land cover dynamics, vegetation recovery, and cloud cover. The Landscape Fire Scars Database for Chile is publicly available in https://doi.org/10.1594/PANGAEA.941127 (Miranda et al., 2022).

Published by Copernicus Publications.

## 1 Introduction

Wildfires, as a natural phenomenon, have been a key component of the terrestrial system for millions of years, shaping biome structure and composition as well as influencing the Earth system's cycles. Human activity has dramatically modified natural wildfire regimes and is now the main driver of their spatial and temporal patterns (Balch et al., 2017; Bowman et al., 2011). The changing fire regime has become an increasing threat to biodiversity (Kelly et al., 2020), agricultural and timber production (Stougiannidou et al., 2020; de la Barrera et al., 2018), and rural/peri-urban communities (Radeloff et al., 2018); it has also become a major contributor to greenhouse gas emissions (Giglio et al., 2013). Recent estimates point to a global mean burned area of 337 to 423 Mha every year (Giglio et al., 2013, 2018). However, the geographical and temporal patterns of fire regimes and their trends over time vary locally depending on the source of ignition (Ganteaume and Syphard, 2018); climate characteristics and their changes (Jolly et al., 2015; Duane et al., 2021); predominant land use and land cover (Butsic et al., 2015); railroad density (Amato et al., 2018); and firefighting, fire suppression and fire prevention capacity (Bowman et al., 2011; Moritz et al., 2014). Additionally, each natural or anthropogenic forcing factor differs in its impact on fire regime attributes (e.g., ignition, severity, burned area and intensity) across multiple spatial and temporal scales worldwide (Ager et al., 2014; Balch et al., 2017; Fusco et al., 2016). An understanding of fire regimes at a local level requires high-resolution, systematic and dynamic databases in order to transform evidence into decision-making in these rapidly changing landscapes (Bowman et al., 2020).

Remote sensing provides the pre-, during and post-fire biophysical information necessary for conducting fire-risk assessment, fire detection and monitoring, assessment of fire impacts, and follow-up of changes in land cover trends after fire occurrence (Szpakowski and Jensen, 2019). Recent public datasets and products have enabled a better understanding of global and regional wildfire patterns (Giglio et al., 2016, 2018; Schroeder et al., 2014; Lizundia-Loiola et al., 2021). Although the principal active fire and burned area products contain information going back to the year 2000 (e.g., MODIS) with a spatial resolution in the best cases of more than 250 m (Chuvieco et al., 2018), there is still a lack of high-resolution wildfire data, especially for developing countries (Chuvieco et al., 2019). Andela et al. (2019) created a global dataset for the period from 2003 to 2016 that estimates the size, duration and propagation rate of individual wildfires with a spatial resolution of 500 m using MODIS products. Likewise, Artés et al. (2019), also using MODIS products, developed a global dataset to analyze fire regimes and fire behavior based on ignition dates and daily burned areas for individual wildfires. The large discrepancies between local and global estimates of burned area occur mostly in the case of fires of less than 100 ha due to detection difficulties when using coarse-resolution products (Roteta et al., 2019; Ramo et al., 2021). This constitutes a significant barrier to the proper understanding of local wildfire regimes and highlights the need for a high-resolution wildfire database (Chuvieco et al., 2019). Recent efforts using Landsat images have led to the identification of annual burn probabilities per pixel from which a database with a 30 m spatial resolution has been constructed that reaches back to the 1980s, but this has been done only for developed countries such as the USA and Australia (Goodwin and Collett, 2014; Hawbaker et al., 2017). However, recent computational advances and the free availability of satellite imagery catalogs provide a promising framework for mapping annual burned areas worldwide, at a spatial resolution of 30 m with Landsat and at a 20 m resolution with Sentinel-2, which would be a major step forward in high-resolution wildfire database generation (Long et al., 2019; Ramo et al., 2021).

In the case of Chile, the fire regime has been described mainly on the basis of the public wildfire database maintained by the Chilean Forest Service (CONAF) as well as with MODIS monthly burned area data, the latter of which have been used only in the most recent studies (de la Barrera et al., 2018; McWethy et al., 2018). Evidence regarding burned areas and fire frequency is derived from data with spatial resolutions between 500 m and 5 km (Gómez-González et al., 2019; González et al., 2018). From these large-scale datasets, it has been determined that fire frequency is closely related to human footprint zones, such as cities or other densely populated areas (Gómez-González et al., 2019; McWethy et al., 2018), roads (Miranda et al., 2020), and agricultural or industrial forest plantation activities (Gómez-González et al., 2019; McWethy et al., 2018). However, burned area also strongly interacts with climatic conditions favorable to the spread of fires, especially warmer and dryer years associated with the El Niño–Southern Oscillation, wet winters the year previous (Holz et al., 2017; Urrutia-Jalabert et al., 2018) and severe drought (González et al., 2018). Such conditions have been more prevalent and more frequent in recent years, with increasing temperatures and a general reduction in precipitation reported for the area since 1980 and a prolonged "megadrought" since 2010 (Boisier et al., 2016; Garreaud et al., 2019). Fire ignition near human communities, favorable climatic conditions, and a lack of landscape or fuel management lead to increased wildfire occurrence (Úbeda and Sarricolea, 2016). However, this large-scale understanding may still be insufficient, especially for local applications such as fire spread modeling, fire severity estimation, landscape planning and design, ecological impacts and ecosystem resilience, or national greenhouse gas emission estimation.

An excellent opportunity for developing countries to generate their own local and historical high-resolution databases of wildfire scars is provided by the Google Earth Engine (GEE) (Long et al., 2019). GEE is an open cloud-computing platform for geospatial analysis that contains a

public catalog of satellite images, topography, land cover and other environmental datasets (Gorelick et al., 2017). Taking advantage of this big-data analysis platform, we generate a detailed database of fire scars in Chile through the development of a flexible workflow, enabling us to reconstruct individual burned areas and fire severity information for all reported historical fires. The result is our Landscape Fire Scars Database for Chile; this database and the GEE script (JavaScript) used to generate it are publicly available at https://doi.org/10.1594/PANGAEA.941127 and https://code.earthengine.google.com/554027d16823525d890ab2f6c45167d9 (last access: 27 July 2022), respectively. This framework could be implemented for any geographical area globally, requiring only that it be adapted to local conditions with respect to seed data availability, fire regimes, land cover or land cover dynamics, vegetation recovery, and cloud cover.

## 2 Data and methods

### 2.1 Study site

The approach that we developed was applied to central and southern central Chile (29–43°5′ S), a long stretch of territory encompassing 10 of the country's administrative regions ($\sim 255\,120\,km^2$). Fire activity in Chile is concentrated in this area, where considerable changes in land use and land cover have been observed in recent decades (Miranda et al., 2017), associated with increased fire activity (González et al., 2018).

### 2.2 Data seeding

To construct our historical database of fire scars, we used a subset of the public wildfire database provided by the Chilean Forest Service (Corporación Nacional Forestal – CONAF). This agency records and stores information on the location, date, cause, affected area by land use, date and time of first control and suppression of fire, among other variables, on all fires (> 0.01 ha). The georeferencing system used by CONAF until 2003 assigned each fire to the center of a 1 km × 1 km alphanumeric grid, based on the subdivision of 1 : 50 000 scale Military Geographic Institute (IGM) maps. After 2003, the location of each fire and estimation of their burned area began to be carried out with the help of Global Positioning System (GPS) information. Given the image availability, quality and spatial resolution of the Landsat programs, we extracted data only for fires with a burned area of more than 10 ha between 1985 and 2018 ($N = 13\,603$). The 10 ha cutoff threshold was chosen because those fires represent more than 93 % of the burned area according to the CONAF official information for the 1985–2018 period. In addition, small fires are usually confounded with agricultural burning, a traditional cultural practice done by Chilean farmers. The original CONAF point dataset is included in our database.

### 2.3 Fire scar generation

Our database was generated using JavaScript programming. The detailed workflow of the script developed to create individual fire scars is shown in Fig. 1. It consists of the following consecutive steps: (i) input data selection and identification; (ii) pre- and post-fire image elaboration; (iii) index, mask calculation and vectorization; (iv) spatial and spectral filtering; and (v) output data generation and export. As noted earlier, we have made the GEE script available to all users as a tool that can be adapted to local conditions and used for permanent database updating. The code is available at https://code.earthengine.google.com/554027d16823525d890ab2f6c45167d9 (last access: 27 July 2022).

The input data in Step (i) must be in point data form with geographic coordinates representing the ignition point or a point within the burned area. The points must indicate the fire start date, the fire control date (fire spread end date) and the estimated burned area. In the absence of the last two pieces of information, we used the fire start date and a fixed burned area of 100 ha as seed values for the initial assessment. The input seed data are converted into a list to process and extract individual fire scars. Around each input point, a circular buffer area is created as a function of the estimated burned area, with the precise dimensions given by $\text{Bufferradius} = \log(\text{burnedarea}) \cdot 2000$. The buffer area is defined because we may only have the fire's ignition point as a spatial reference. Therefore, it is necessary to explore the area near this point to find the limits of the fire scar. This could be an interactive process depending on the burned area or the shape of the fire scar.

In Step (ii), two image collections (sets of images) are prepared for each wildfire, depending on the fire start date. We use the atmospherically corrected surface reflectance and orthorectified images from Landsat 5 – "LANDSAT/LT05/C01/T1_SR" (1984–2013), Landsat 7 – "LANDSAT/LE07/C01/T1_SR" (1999–2021), and Landsat 8 – "LANDSAT/LC08/C01/T1_SR" (2013–present), with one image collection for a pre-fire condition and another for a post-fire condition, all of which are available from the GEE. To avoid conflicts in mathematical operations for pre- and post-image collection generation, the date in day/month/year format is converted to Unix time format, which represents the number of milliseconds that have elapsed since January 1970. Based on the fire start and control dates, the respective image searches for both pre-fire and post-fire events are each conducted for a period of 100 d. If this proves insufficient to get at least one image, the period can be extended up to 2 years for a pre-fire event and up to 6 months for a post-fire event. However, a definition of the maximum period of time must be chosen considering the local phenology, vegetation recovery or landscape dynamics, which are aspects that could change the spectral response of the land surface after fire. Pixels of snow, clouds and cloud shadows are ex-

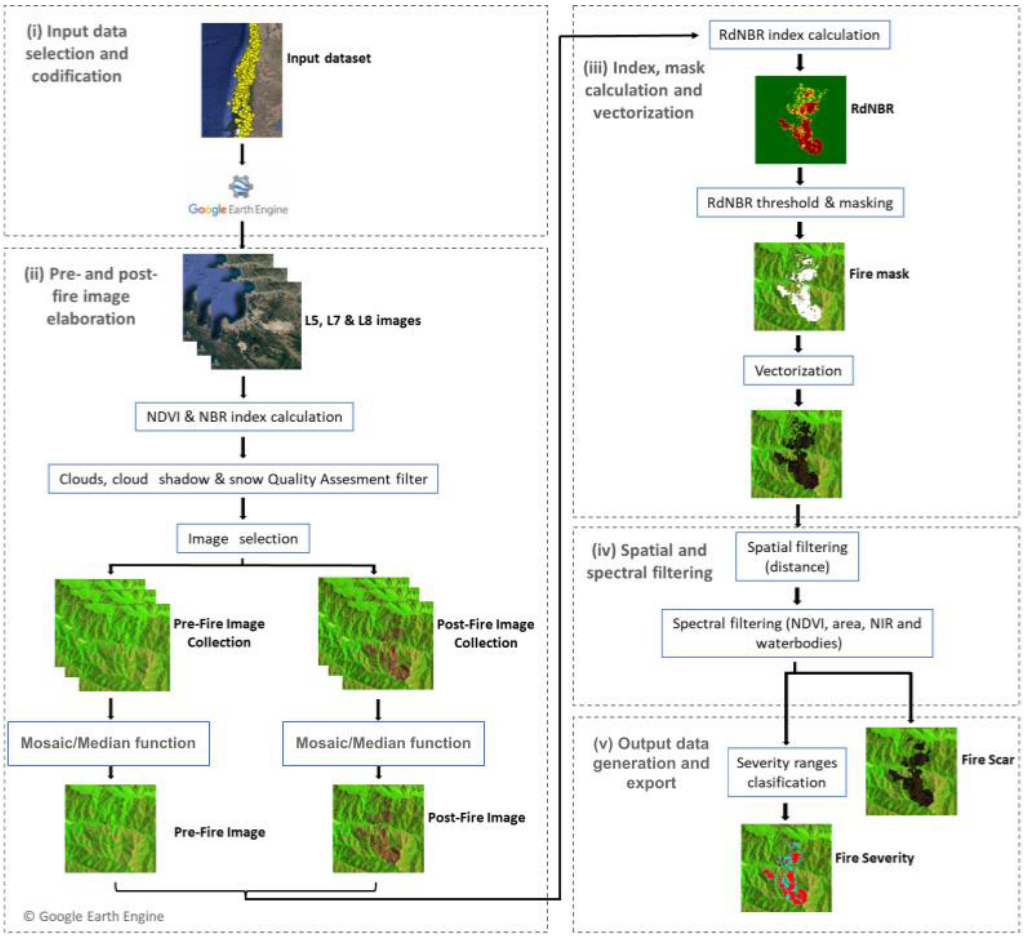


**Figure 1.** Detailed workflow for individual fire scar generation in the Google Earth Engine. See Table 1 for details on the normalized burned ratio (NBR) and the relative delta normalized burn ratio (RdNBR).

cluded from each image on the basis of the pixel quality band provided by Landsat and used as a binary mask of good and bad quality of the surface reflectance. For each image collection, we applied either the "mosaic" or the "median" reducer function to get a unique image of the landscape conditions at moments as close as possible before and after a fire event. This can be done by sorting the image by its date and obtaining the closer good-quality pixels. When the mosaic reducer did not provide good-quality pixels, we applied the median reducer instead. The median method for reducing image collections avoids extreme values by selecting the median value for each pixel.

Using the final pre- and post-mosaic images obtained as outlined above, we then (in Step iii) calculated all of the spectral indices (Table 1) used to identify the burned and unburned areas. The most widely used burned area index is the normalized burned ratio (NBR) and its multitemporal form, the delta normalized burn ratio (dNBR) (Lentile et al., 2006; Fassnacht et al., 2021). These indexes reduce detection errors caused by shadows, waterbodies, agricultural or tree harvesting, flooding, and snowmelt (Chuvieco et al., 2019; Long et al., 2019). Other burned area indexes have been proposed, and a combination of them may give the best results; however, to discriminate between burned and unburned areas, we opted for the relative delta normalized burn ratio (RdNBR). This index has shown good results in Mediterranean areas (Miller and Thode, 2007).

Step (iv) involved the selection of the RdNBR index value for each wildfire that best captures the burned area based on visual interpretation. This is an interactive (fire-by-fire) process based on visual assessment of the best RdNBR value that delimitates each individual fire scar. The raster mask of the burned area was converted to vector format for spatial and spectral filtering (Fig. 1). By vectorizing the initially identified burned patches, spatial and spectral information could be added to each one so that burned and unburned patches could be better distinguished using new criteria. This information included the mean normalized difference vegetation index (NDVI) both before and after the fire event, the near-infrared (NIR) minimum value after the event, and each patch's calculated area. The information added to the initial burned area patches could help to filter misclassified areas as burned ar-

**Table 1.** Description of the spectral indexes and formulas used in the workflow.

| Index | Abbreviation | Formula | Usage | Reference |
|---|---|---|---|---|
| Normalized difference vegetation index | NDVI | $\frac{\rho\text{NIR}-\rho\text{RED}}{\rho\text{NIR}+\rho\text{RED}}$ | Detects pre- and post-fire vegetation cover | Rouse et al. (1974) |
| Normalized burned ratio | NBR | $\frac{\rho\text{NIR}-\rho\text{SWIR2}}{\rho\text{NIR}+\rho\text{SWIR2}}$ | Detects burned areas | Key and Benson (2003) |
| Delta normalized burn ratio | dNBR | PreFireNBR − PostFireNBR | Detects changes in the NIR and SWIR bands to identify burned area and fire severity | Key and Benson (2003) |
| Relative delta normalized burn ratio | RdNBR | $\frac{\text{PreFireNBR}-\text{PostFireNBR}}{\sqrt{\text{ABS(PreFireNBR)}}}$ | Normalizes changes by pre-fire vegetation condition | Miller and Thode (2007) |

NIR stands for near infrared, and SWIR represents short-wave infrared.

eas, thereby reducing commission errors. We also calculated the NDVI in order to estimate several vegetation parameters based on the red and infrared spectral bands (Table 1). The NDVI can be used to represent the current state of the composition, structure and phenology of vegetation as well as plant health and even burned vegetation; it can also be used to represent the changes over time in the abovementioned parameters (Helman, 2018; Pettorelli et al., 2005). Spatial filtering begins by defining an initial search distance to the ignition point of 1 km, although this distance can be interactively defined or modified later. The biggest patch within that distance is then identified, and a new distance from this patch is defined. Only the patches within this latter distance are considered. At this stage, polygons or patches that may cause commission errors are eliminated from the areas counted as burned in the preliminary mask. They may include (a) waterbodies with a pre-fire mean NDVI of less than 0.1, (b) polygons or patches for which the pre-fire mean NDVI is less than 0.1 (denoting a lack of vegetation), and (c) other filtering criteria similar to those proposed by Long et al. (2019). Each polygon or patch that satisfies the filtering criteria and has a minimum area of 0.3 ha is retained. The filter values can be changed to suit local conditions.

Finally, in Step (v), once the fire scar is delimited, the event's severity is calculated from the RdNBR in a continuous raster format and categorized based on the severity category ranges proposed by Miller and Thode (2007): unchanged ($< 69$), low (69–315), moderate (316–640), and high ($\geq 641$). Our database also makes available the pre- and post-fire NBR index for each image. Each fire scar and its severity are exported in vector and raster format, along with the multispectral corrected Landsat images of pre- and post-fire events and the RdNBR index. The vector data contain information about the fire record, the calculated area and the spectral responses used for filtering. The output name of each vector and raster file is OBJECT (FireScar, Severity, ImgPre, ImgPost and RdNBR) +_ISO-REGION_ID +_u-THRESHOLD RdNBR VALUE +_START DATE, where ISO-REGION is the name of the administrative region based on the ISO 3166-2:CL norm; ID is the identification number of the evaluated fire; THRESHOLD VALUE is the numerical value of the RdNBR index used to separate burned and unburned areas; and START DATE is the date used to find the first image previous to the fire, which will be the same as the fire start date in day/month/year format (e.g., FireScar_CL-RM_ ID1920451_u330_19990215) in most cases. A detailed description of each variable and its format is included as supplementary material in the database metadata.

### 2.4 Fire scar evaluation

We compared our fire scars with those generated by CONAF for the 2015–2016, 2016–2017 and 2017–2018 fire seasons and published in Brull (2018). The aforementioned publication elaborated on a manual digitalization of the fire scar perimeters using secondary information such as pre- and post-fire Landsat satellite images, the dNBR index, Visible Infrared Imaging Radiometer Suite (VIIRS) active fire data, and Sentinel 2 images for high-resolution interpretation. The fire perimeters were defined as the outer limit between the burned and unburned area in the landscape, but the unburned areas inside this perimeter were not discounted in the final fire scars. Brull (2018) generated 194 fire scars, of which 78 coincided with two criteria for making comparisons: (i) an individual fire scar must be at a distance of at least 300 m from another reported fire (by Brull, 2018), and (ii) the fire must have the same name, start date and control as our seed data in order to avoid confusion. From 194 fire scars collected by Brull (2018), 107 were within 300 m of another reported fire, and the name and dates of fires did not match for 9 fire scars. The mean area of the remaining 78 fire scars was 1180 ha (minimum area of 200 ha and max area of 12 250 ha). In order to avoid confusion between fire events, the evaluation was carried out for individual fires located at least 300 m from any other scar from the same season (according to the date). The evaluation of the 78 fire scars itself was based on

the index proposed by Singh et al. (2015) that compares two georeferenced polygons using the closeness index ($D$):

$$D(i,j) = \sqrt{(\text{OverSegmentation}(i,j))^2 + (\text{UnderSegmentation}(i,j))^2}, \quad (1)$$

where $i$ is the reference polygon, $j$ is the segment polygon, OverSegmentation $(i,j) = 1 - \frac{A_{\text{intersect}}(i,j)}{A_{\text{reference}}(i)}$, and UnderSegmentation $(i,j) = 1 - \frac{A_{\text{intersect}}(i,j)}{A_{\text{segment}}(j)}$. Here, $A_{\text{intersect}}(i,j)$ is the common area between segment polygon $j$ and the corresponding reference polygon $i$, $A_{\text{reference}}(i)$ is the area of reference polygon $i$, and $A_{\text{segment}}(j)$ is the area of segment polygon $j$.

In order to normalize the values of $D$, we use the modification form $D_{\text{norm}} = 1 - \left(\frac{D}{\sqrt{(2)}}\right)$, where $D_{\text{norm}}$ is the normalization of $D$ values between zero (non-matching polygons) and one (perfectly matching polygons).

To assess the accuracy of our framework, we include the evaluation of commission and omission error calculated as follows: commission error = FP/(FP+TP), and omission error = FN/(FN+TP). Here, FP is the spatial explicit false positive area of the generated fire scar compared with the reference polygon of Brull (2018), FN is the false negative area and TP is the true positive area.

### 2.5 Database quality control

Even though the data generation process is done with standard and stable GEE scripts, the project's enormous scope could lead to involuntary discordances in resulting files. A thorough revision was performed over approximately 140 000 files, considering the three following major areas: (i) file and layer naming, file readability and type and amount of files per fire scar; (ii) geographic locations and burned-area-related revision; and (iii) dates and season-related revision. The approach was to define several tests regarding relations between the content and attributes of the files in each area that the whole dataset should comply to. The revision scripts were written in Python in the Google Colab environment, with direct access to the Google Drive files generated by the GEE process. The tests were written for our resulting database, but they are generic in most terms and assumptions and are available at https://github.com/cr2uchile/Quality_Control_FireScarCL (last access: 28 July 2022). Some of these tests led to human revision of the fires, either regenerating them or removing them from the fire scar database, and other tests led to automated fixes, like name change or attribute column and content changes in the vector files. The resulting database of 8153 fire scars complies with the following statements:

- All fires have a unique identifier and 17 related files, including two satellite composite raster .tif images that cover a domain larger than the identified fire scar and merge pre- and a post-fire images (ImgPreF.tif and ImgPosF.tif, respectively); three respective raster .tif images with the shape of the fire scar that contain (1) zeroes where there is no fire scar identified and ones where a fire scar is identified (FireScar.tif), (2) zeroes where there is no fire scar identified and severity index values (from one to three) to identify the severity where there is a fire scar (Severity.tif), and (3) the RdNBR value (float numbers) for the points where there is a fire scar (RdNBR.tif); and, finally, two vector shapefile images that contain six files each (.shx, .shp, .dbf, .cpg, .fix and .prj), where one is the vectorized representation of FireScar.shp, and the other is the vectorized representation of Severity.shp with polygon and attribute information.

- For each set of resulting fire scar files, the ISOREGION_ID corresponds to the region assigned by the original CONAF point dataset, and the START_DATE corresponds to the ignition point assigned by CONAF. This was preserved to better identify the resulting fire scars with the seed database.

- All raster .tif image files have the same area type and coordinate system. All pre and post-fire .tif images have eight readable bands.

- For each fire, the pre- and a post-fire .tif images have the same width and height dimensions and the same exact geographic extent. Moreover, their domain contains the fire scar's ignition point and the resulting raster fire scar .tif images (FireScar.tif, Severity.tif and RdNBR.tif). The FireScar and Severity vector shapefiles files have consistent values in their attribute tables, and the number of polygons of the Severity vector image is equal or more than the number of polygons of the FireScar vector image. The dates in the attribute tables have the format YYYY-MM-DD, and the texts have UTF-8 encoding. Original fire names that included diacritics (e.g., ñ) were replaced by normal characters.

## 3 Results

Using the data for all 12 250 fires recorded by CONAF between 1985 and 2018 with a burned area greater than 10 ha, we were able to reconstruct 8153 fire scars, comprising 66.56 % of the total registered fires (Table 2, Fig. 1). Suitable images were found for 35 % of recorded fires for the period 1985–1994, 63 % of recorded fires for 1995–2004, 82 % of recorded fires for 2005–2014 and 93 % of recorded fires for 2015–2018. The increasing trend evident in these percentages reflects how image availability has grown over time. Smaller numbers of suitable images were found for the country's southern regions (Los Ríos and Los Lagos), the wettest and coldest areas included in our study, where cloud cover is continuous for much of the year (Table 2).

**Table 2.** Regional and temporal distribution of fires and reconstructed fire scars. The administrative regions are those included in the study. The "Number of fires" column indicates the total number of fires recorded by CONAF for which the burned area was over 0.01 ha. "Yes" denotes the number of reconstructed fire scars contained in our database, and "No" denotes the number of fire scars in the database that could not be reconstructed due to the unavailability of satellite images.

| Administrative region | Number of fires | Number of fires > 10 ha | Reconstructed fire scars > 10 ha (%) | Total fire scars 1985–2018 | | Total fire scars 1985–1994 | | Total fire scars 1995–2004 | | Total fire scars 2005–2014 | | Total fire scars 2015–2018 | |
|---|---|---|---|---|---|---|---|---|---|---|---|---|---|
| | | | | Yes | No | Yes | No | Yes | No | Yes | No | Yes | No |
| Coquimbo | 1863 | 238 | 60.92 | 145 | 93 | 27 | 51 | 40 | 24 | 38 | 17 | 40 | 1 |
| Valparaíso | 31 857 | 1784 | 80.38 | 1434 | 350 | 400 | 160 | 352 | 40 | 425 | 140 | 257 | 10 |
| Metropolitana | 15 337 | 1109 | 85.75 | 951 | 158 | 208 | 79 | 252 | 42 | 261 | 33 | 230 | 4 |
| O'Higgins | 8249 | 1221 | 85.09 | 1039 | 182 | 240 | 93 | 251 | 56 | 365 | 26 | 183 | 7 |
| Maule | 14 475 | 1419 | 65.89 | 935 | 484 | 103 | 290 | 199 | 118 | 393 | 52 | 240 | 24 |
| Ñuble and Biobío | 77 704 | 3248 | 58.07 | 1886 | 1362 | 124 | 775 | 473 | 375 | 712 | 171 | 577 | 41 |
| Araucanía | 31 306 | 2369 | 57.41 | 1360 | 1009 | 30 | 458 | 346 | 356 | 424 | 131 | 560 | 64 |
| Los Ríos | 3680 | 339 | 35.99 | 122 | 217 | 8 | 154 | 41 | 48 | 33 | 10 | 40 | 5 |
| Los Lagos | 8416 | 523 | 53.73 | 281 | 242 | 5 | 100 | 53 | 111 | 143 | 27 | 80 | 4 |
| Total | 192 887 | 12 250 | 66.6 | 8153 | 4097 | 1145 | 2160 | 2007 | 1170 | 2794 | 607 | 2207 | 160 |

The total number of fires > 0.01 ha exhibits a positive linear relationship with the total number of fires > 10 ha recorded by CONAF between 1985 and 2018 ($R^2 = 0.86$). The number of recorded fires > 10 ha and the number of reconstructed fire scars per region exhibit the same positive linear relationship ($R^2 = 0.92$), indicating that the distribution of the reconstructed data is regionally representative (Table 2, Fig. 2). However, the pattern of relationships between recorded fires and reconstructed fire scars for the different regions varies from period to period. For 1985–1994, the relationship was weak ($R^2 = 0.1$), but it had strengthened by 1995–2004 ($R^2 = 0.91$); the same pattern could be seen again for 2005–2014 ($R^2 = 0.93$) and 2015–2018 ($R^2 = 0.93$). The definitive version of our database is ordered by region and fire season to facilitate exploration and analysis, revealing, for example, the high levels of fire activity areas near the coastal cities of Valparaíso and Concepción over the various decades (Fig. 3).

For each of the 8153 reconstructed fire scars, our database contains the following: (i) a Landsat mosaic of pre- and post-fire event images (.tif) with eight spectral bands – blue, green, red, NIR, SWIR1 and SWIR2, NDVI, and NBR (Fig. 4); (ii) the raster of the fire scar in binary format (.tif), where one is the burned area and zero is the unburned area (Fig. 4); (iii) the RdNBR index, both in continuous values (.tif) and categorized by severity classification level, where zero is unchanged, one is low severity, two is medium severity and three is high severity (Miller and Thode, 2007) (Fig. 4); and two vector files (.shp) containing (iv) the fire scar perimeter and (v) the fire scar severity classification (Miller and Thode, 2007). Layers of information are assigned to each individual burned patch indicating its size as well as detected fire start and control dates, and spectral data. NBR bands are available for each image in order to enable reassessment of the fire scar and its severity. A detailed description of each variable and its format may be found in the database metadata.

### 3.1 Fire scar evaluation

We evaluated the fire scars reconstructed using our approach by contrasting them with the 78 scars derived from the official CONAF data that were suitable for making comparisons. A perfect match could not, of course, be expected given the differences between the two methodologies. One particularly crucial difference is that the CONAF fire scar digitalization includes patches that were actually not burned within the fire perimeter for each fire event. These patches constituted anywhere from 13.5 % to 18.2 % of the area indicated as burned, depending on the fire season (Brull, 2018). Moreover, the CONAF digitalization was complemented by the agency's own fieldwork, which improved the detection of low-severity fires or surface fire under the canopy. Nevertheless, the global accuracy assessment, derived from the closeness index and calculated as the mean of the individual $D_{\text{norm}}$, resulted in a value of 0.79. Examples of the comparisons of our reconstructed fire scars with CONAF data reported by Brull (2018) are shown in Fig. 4 along with the respective $D_{\text{norm}}$ index for each case. Finally, we found a commission error of 7 % and an omission error of 28 %.

### 3.2 Limitations and other observations regarding the Landscape Fire Scars Database

The following points outline the limitations of our Landscape Fire Scars Database as well as other pertinent observations:

1. Our Landscape Fire Scars Database does not represent all of the fires recorded in the 1985–2018 period.

2. The reconstructed fire scars are mainly concentrated in the last 20 years of the abovementioned period, which may be related to the improvement in image availability over time .

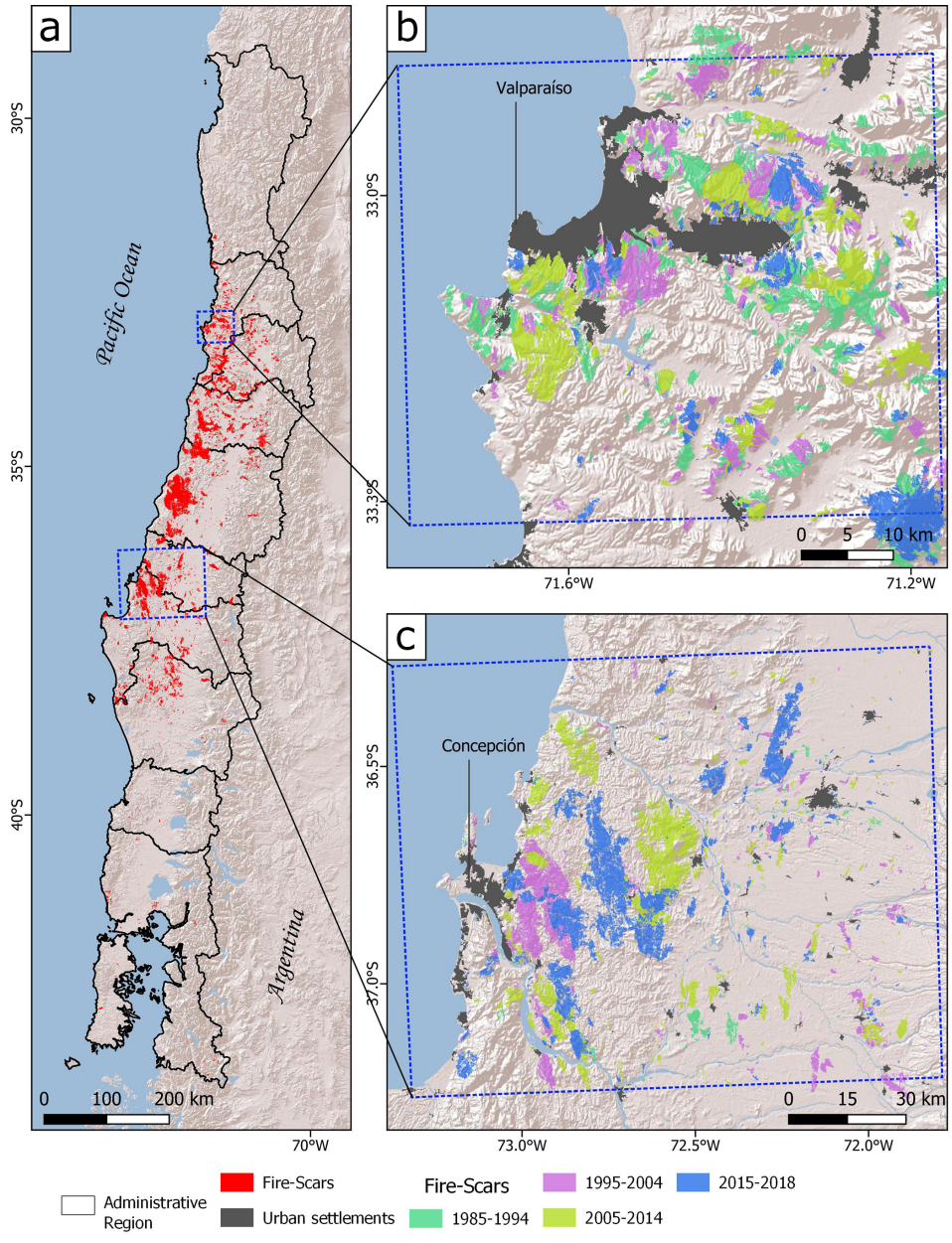


**Figure 2.** Panel **(a)** shows the geographic distribution of the fire scar database, and panels **(b)** and **(c)** show examples of fire activity near the cities of Valparaíso and Concepción for different periods.

3. Remotely sensed fire severity estimates the change in the spectral response in the burned area and must be carefully treated in the analysis of fires' ecological impact. Low-severity or surface fire may be underestimated.

4. Due to the 16 d interval between Landsat images, one fire scar reconstructed from them may represent more than one fire event in neighboring areas experiencing multiple fires over that interval, especially in the case of originally independent fire events that may have merged. Thus, some fire scars in the database may be duplicated if they merged with another fire due to their proximity in space and time. We include a notification in the database where this could have happened.

5. Commission errors may occur due to other land cover changes such as tree plantation clear-cutting or harvesting of crops.

6. In certain cases, the inclusion of additional available images of pre- and post-fire events may help to improve the fire scars.

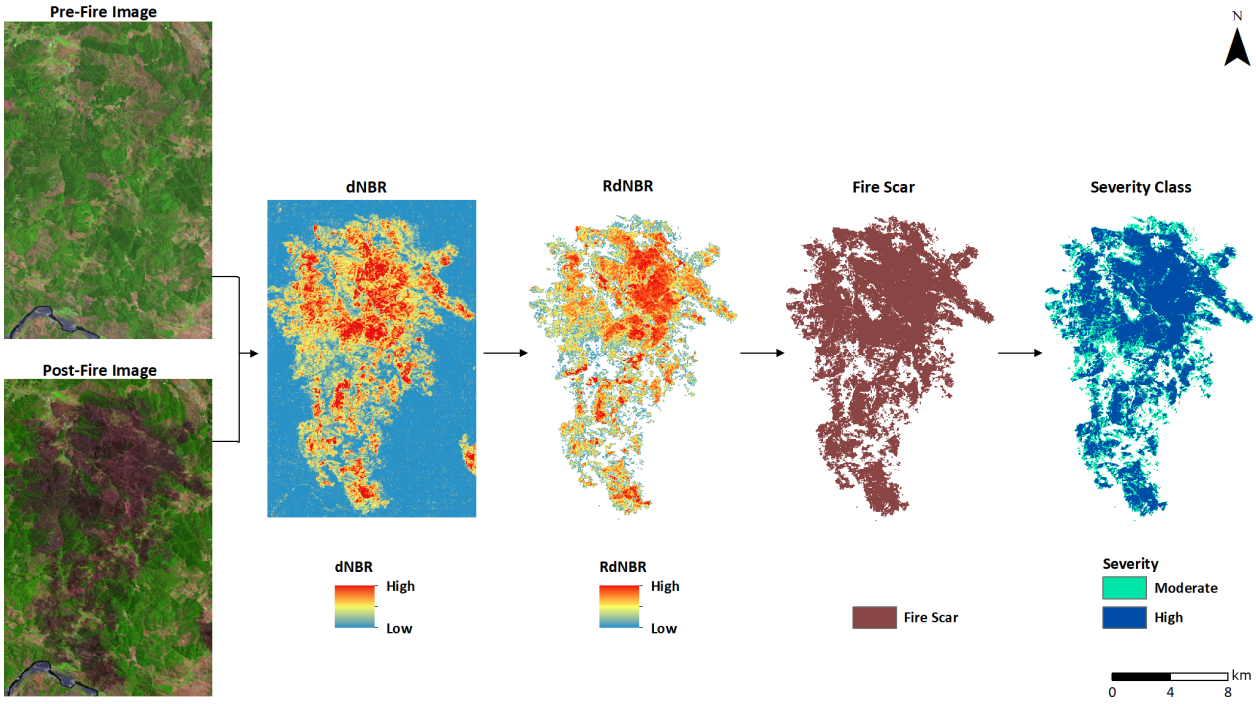


**Figure 3.** The database content for each reconstructed fire scar. See Table 1 for details on the dNBR and RdNBR. The illustrated event is from the Maule region and occurred in 2014.

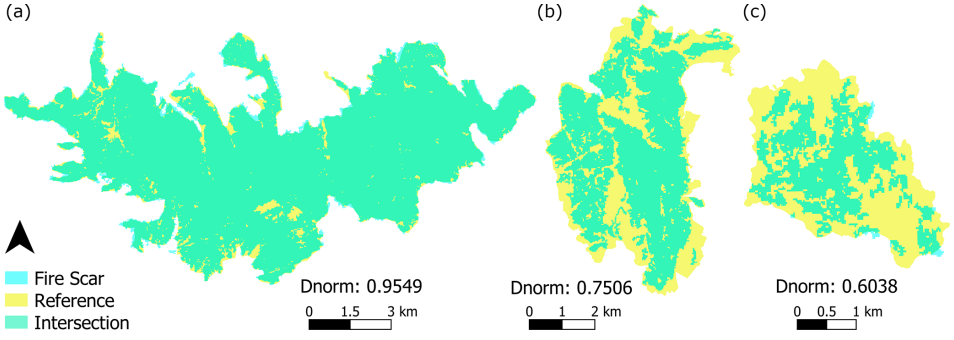


**Figure 4.** Evaluation of the fire scars. Shown are three examples comparing fire scars from CONAF with the images reconstructed using our Landscape Fire Scars Database methodology. See Sect. 2.3 for a detailed description of Dnorm.

## 4 Data availability

The Landscape Fire Scars Database for Chile can be downloaded from the PANGAEA repository at https://doi.org/10.1594/PANGAEA.941127 (Miranda et al., 2022).

## 5 Discussion and conclusions

The creation of our Landscape Fire Scars Database for Chile makes a high-resolution individual burned area product for the country publicly available for the first time. The georeferenced database is a multi-institutional effort containing information on more than 8000 fire events between 1984 and 2018 that affected an area of over 10 ha. It contains data on fire scar area, perimeter and severity, which are accessible to the general public for analyzing future changes, improvements and new evaluations. Furthermore, the methodology for generating these data was implemented in GEE so that others may replicate our approach or apply it to other countries or cases where no openly accessible datasets are currently available. Public institutions and researchers can take advantage of this framework to generate long-term time series of fire scars for any years of interest or just for one particularly significant wildfire. The international community can replicate this workflow using national fire occurrence data with the minimum required information or with recently released data on ignition coordinates, date and fire duration for more than

13 million individual fires worldwide that occurred between 2003 and 2016 (Andela et al., 2019). As a high-resolution fire scar database, the Landscape Fire Scars Database should be of much help in conducting accurate and systematic evaluations of underlying wildfire forces, impacts and recoveries as well as in delineating populations and biodiversity, public policy, and informed territorial decision-making and planning (Chuvieco et al., 2019; Long et al., 2019; Stenzel et al., 2019).

Creating this database based on information distributed over an extensive territory at a national scale using a single method presented diverse challenges with respect to (i) historical image availability, (ii) land cover and land cover change dynamics, (iii) temporal image resolution and image cloud cover, and (iv) seeding datasets. In what follows, each of these issues is discussed in turn.

i. Historical image availability

GEE (https://earthengine.google.com, last access: 28 July 2022) provides free online access to original and corrected Landsat program data and products. Users do not need to download the images, and the analysis and image modification are also carried out online, powered by Google servers (Gorelick et al., 2017). Image availability in the Landsat program is rather uneven across countries, with those in the developing world generally less well represented in terms of historical records. Nevertheless, the continuity of the image time series improves noticeably as the time period in question approaches the present. In the case of Chile, this pattern of improvement is clearly evidenced in the fire scar generation success rates that we obtained for time periods since the mid-1980s (1985–1994: 35 %; 1995–2004: 63 %; 2005–2014: 82 %; 2015–2018: 93 %), which are consistent with the availability of cloud-free pixels for the country (Fig. 5). This tendency must be considered when determining the time periods used to reconstruct a database for any specific region. For example, according to the Landsat Global Archive Consolidation updates (Wulder et al., 2016), availability and usable image quality are lower for Southern Hemisphere high-latitude regions (Huang et al., 2010; Stillinger et al., 2019; Viale et al., 2019).

ii. Land cover and land cover change dynamics

Almost 90 % of wildfire ignitions and burned areas worldwide have anthropogenic origins (Ganteaume and Syphard, 2018). As a result, many of these fires impact the wildland–urban interface, urban and rural settlements, and productive regions (e.g., agricultural lands and tree plantations). Zones with high rates of land use or land cover change may present some difficulties in fire scar and severity mapping. Remotely sensed burn area indexes are based on the abrupt change in the pre-fire spectral band values following a fire event. For example, NBR uses the near-infrared (NIR) and shortwave infrared (SWIR) bands as proxies for the photosynthetic productivity and water content of vegetated areas (Lentile et al., 2006; van Wagtendonk et al., 2004). Both parameters are affected by fire; thus, the greater the temporal difference in the index, the greater the event's severity. However, the spectral response of those bands may also be influenced by other factors. Forestry activity, especially tree plantation clear-cutting, deforestation or harvesting on agricultural land as well as the drying of annual grassland in the summer season, dried meadows and the cultural practice of burning agricultural wastes may all act to confuse the spectral response for a given landscape, assimilating them to wildfire (Ghermandi et al., 2019). Another local consideration is the recovery rate of the vegetation. For example, recovery is faster in the tropics than in temperate areas, which could affect the mapping of burned areas or fire intensity estimation depending on how much time has passed between fire occurrence and the acquisition of a good-quality satellite image (Chuvieco et al., 2019). Local topography may also complicate the process of distinguishing burned areas in mountainous zones due to the increased presence of shadows, fog or melting snow in cold or high-elevation areas (Huang et al., 2010; Stillinger et al., 2019; Viale et al., 2019). Therefore, local experience in landscape dynamics and practice is crucial to ensuring the generation of accurate databases and may constitute a basis for adapting the most commonly used burned area indexes to local realities.

iii. Temporal image resolution and image cloud cover

Landsat images are widely used to study land cover changes and trends due to their spatial and temporal resolution (Soulard et al., 2016). However, the 16 d interval between images could be a major limitation. In regions with high fire activity, this can make it more difficult to identify individual fire scars and differentiate them from those produced on other days in neighboring locations. This means that a single final fire scar may in fact have been created by multiple fire events occurring over the 16 d period that converged or totally fused. This problem could be mitigated by using Sentinel-2 images (also available in GEE) for the earliest fire events, given that the Sentinel-2 program is available from mid-2015 with a temporal resolution of 5–6 d (starting in 2017) and a pixel size of 10 and 20 m (e.g., SWIR band), although the increased spatial resolution may raise another issue in that it could result in the underestimation of the influence of dead vegetation shadows on the spectral index signals (Fassnacht et al., 2021). The high temporal resolution could also be helpful in zones with high cloud cover such tropical and high-latitude or mountainous areas (King et al., 2013). For example, we observe that the Landsat archive in Africa could reduce its number

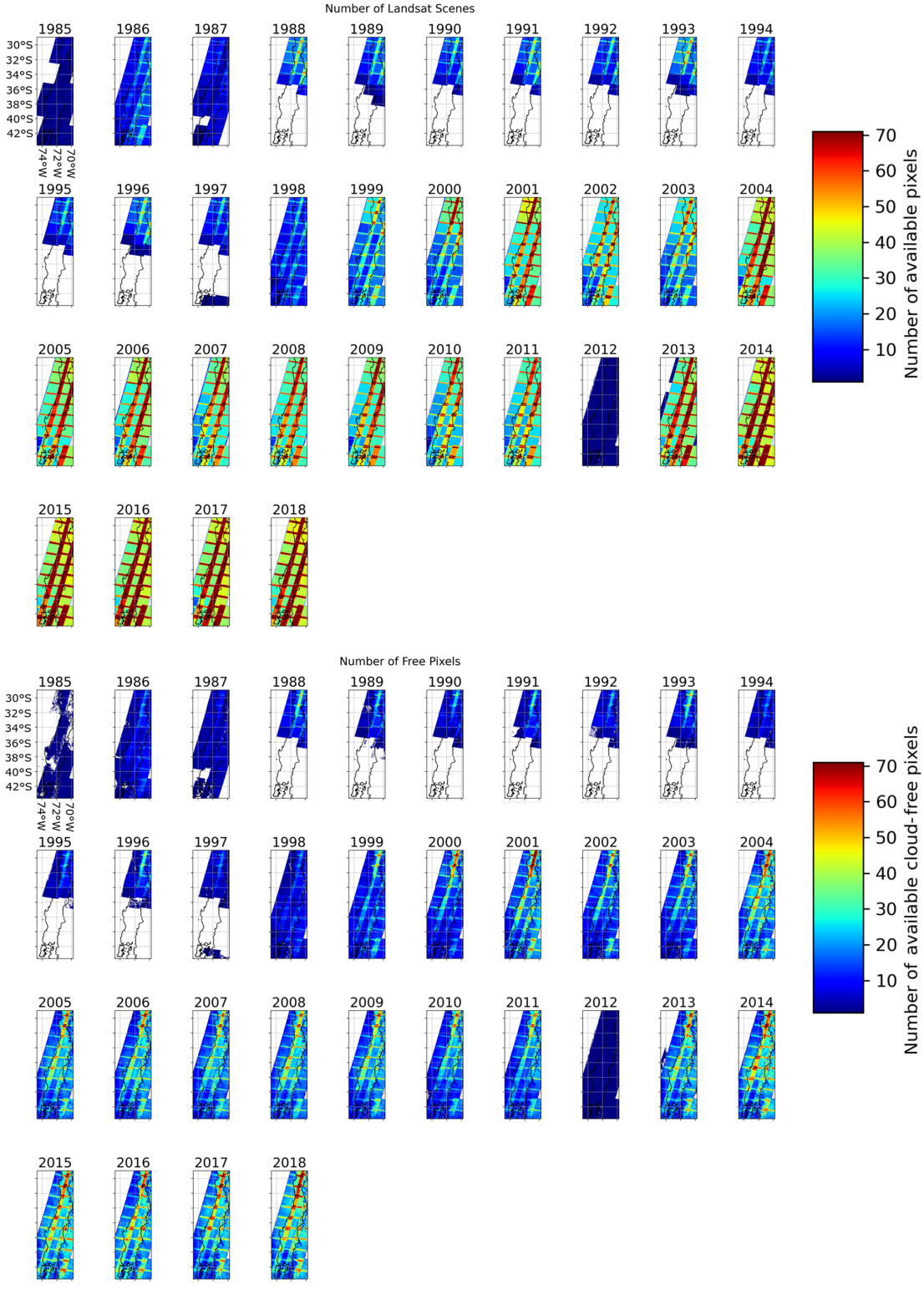


**Figure 5.** The upper set of panels shows the available Landsat pixels over study area for each respective year from 1985 to 2018. The lower set of panels represents the number of available cloud-free Landsat pixels per year for the same respective years.

of cloud-free images (images with less than 40 % cloud cover) to a mean of 25 %, with much fewer images in the tropical zone of the Congo Basin (Roy et al., 2010).

The RdNBR index is able to differentiate burned area from non-burned area over a diverse range of climatic and geographic conditions. No evident pattern associated with the latitudinal or vegetation-type change was observed when applying the threshold value to identify scars. In general, RdNBR performs wells when compared with field plots of severity. It is little influenced by the type of forest and is determined mainly by the fraction of consumed canopy cover (Cardil et al., 2019; Soverel et al., 2010; Fassnacht et al., 2021), demonstrating the index's high versatility. Nevertheless, the task of assessing the performance of the severity classification is left to users of the database, and it will depend on the local land cover context and field validations for identification of the best index. Our database does provide the NBR band for the images in order to facilitate a comparison and evaluation of the dNBR and RdNBR indices.

The importance of the proposed database also stems from its value as an input source for methods based on artificial intelligence (AI) aimed at automating the process of generating new fire scars. AI techniques (such as machine learning, ML; deep learning, DL; and, especially, the convolutional neural network, CNN) are increasingly being used for classification or object segmentation problems (Alzubaidi et al., 2021). The integration of such methods with remote sensing data is enabling the development of burned area detection models that use manually (user-) delimited wildfire perimeters as their training dataset. Promising results have been achieved using uni- or multi-temporal images and different types of remote sensing data to address the many open challenges in wildfire mapping and monitoring (Hu et al., 2021; Knopp et al., 2020; Pinto et al., 2021).

In conclusion, we believe that the present study makes a significant contribution to the development of high-resolution methods for mapping fire scars and their temporal and spatial patterns. Our hope is that it will serve as the first step in an ongoing effort to build and maintain an extensive, consistent database on forest fires in Chile that will drive scientific research and improvements in landscape management. Further study is needed to broaden the current state of knowledge on local conditions through standardized field surveys.

iv. Seeding datasets

Studies in Chile have previously evaluated the performance of the global satellite burned area products showing good performance. A spatial resolution improvement of those products can be done using the fires detected by global datasets in Chile or another area as the seed point. Global datasets such as MODIS Collection 6 burned area data, MCD64A1 (Giglio et al., 2009); VIIRS active fire data (Schroeder et al., 2018); and Global Fire Atlas data (Andela et al., 2019; Giglio et al., 2018) can be used to evaluate the performance of our approach for medium and large fires and to create new high-resolution datasets for mapping fire scars in different ecosystems and under different land cover conditions.

**Author contributions.** AM, RM, IM, MEG, AL, IC and MG designed the study and database and were responsible for funding acquisition. AM and RM managed the project and wrote the original draft of the paper with contributions from all co-authors. AM, RM, GA, LA, DB, MB, SB, PC, FC, GC, FdlB, CH, IM, CO, FP, RR and VU carried out the image interpretation, data processing and development of databases as well as providing different input on the manuscript and database. FM was responsible for the data curation and database quality control.

**Competing interests.** The contact author has declared that none of the authors has any competing interests.

**Disclaimer.** Publisher's note: Copernicus Publications remains neutral with regard to jurisdictional claims in published maps and institutional affiliations.

**Acknowledgements.** Alejandro Miranda, Antonio Lara, Mauricio Galleguillos, Mauro González and Francisca Muñoz acknowledge funding from ANID/FONDAP (grant no. 15110009), and Alejandro Miranda is grateful to the ANID postdoctoral Fondecyt project (grant no. 3210101) and FONDEF-IDEA (grant no. ID20I10137) for financial support. The authors also wish to thank the Complex Engineering Systems Institute PIA/BASAL (grant no. AFB180003). Mauro E. González is grateful to ANID/-Fondecyt (grant no. 1201528) and the Center for Fire and Socioecosistem Resilience (FireSES). The authors thank the Corporación Nacional Forestal (CONAF) for providing the seeding and digitalized fire scar data for database evaluation; they also wish to give special thanks to Jordi Brull and the hundreds of anonymous firefighters and professionals who have observed, surveyed and developed the CONAF official fire records since 1984. Finally, the authors wish to acknowledge the Chilean Institute for Disaster Resilience (ITREND) for their support.

**Financial support.** This research has been supported by ANID/-FONDAP (grant no. 15110009), ANID/Fondecyt (grant no. 3210101), FONDEF-IDEA (grant no. ID20I10137), PIA/BASAL (grant no. AFB180003) and the Center for Fire and Socioecosystem Resilience.

**Review statement.** This paper was edited by Sander Veraverbeke and reviewed by three anonymous referees.

## References


Ager, A. A., Preisler, H. K., Arca, B., Spano, D., and Salis, M.: Wildfire risk estimation in the Mediterranean area: MEDITERRANEAN WILDFIRE RISK ESTIMATION, Environmetrics, 25, 384–396, https://doi.org/10.1002/env.2269, 2014.

Alzubaidi, L., Zhang, J., Humaidi, A. J., Al-Dujaili, A., Duan, Y., Al-Shamma, O., Santamaría, J., Fadhel, M. A., Al-Amidie, M., and Farhan, L.: Review of deep learning: concepts, CNN architectures, challenges, applications, future directions, J. Big Data, 8, 53, https://doi.org/10.1186/s40537-021-00444-8, 2021.

Amato, F., Tonini, M., Murgante, B., and Kanevski, M.: Fuzzy definition of Rural Urban Interface: An application based on land use change scenarios in Portugal, Environ. Model. Softw., 104, 171–187, https://doi.org/10.1016/j.envsoft.2018.03.016, 2018.

Andela, N., Morton, D. C., Giglio, L., Paugam, R., Chen, Y., Hantson, S., van der Werf, G. R., and Randerson, J. T.: The Global Fire Atlas of individual fire size, duration, speed and direction, Earth Syst. Sci. Data, 11, 529–552, https://doi.org/10.5194/essd-11-529-2019, 2019.

Artés, T., Oom, D., de Rigo, D., Durrant, T. H., Maianti, P., Libertà, G., and San-Miguel-Ayanz, J.: A global wildfire dataset for the analysis of fire regimes and fire behaviour, Sci. Data, 6, 296, https://doi.org/10.1038/s41597-019-0312-2, 2019.

Balch, J. K., Bradley, B. A., Abatzoglou, J. T., Nagy, R. C., Fusco, E. J., and Mahood, A. L.: Human-started wildfires expand the fire niche across the United States, P. Natl. Acad. Sci. USA, 114, 2946–2951, https://doi.org/10.1073/pnas.1617394114, 2017.

Boisier, J. P., Rondanelli, R., Garreaud, R. D., and Muñoz, F.: Anthropogenic and natural contributions to the Southeast Pacific precipitation decline and recent megadrought in central Chile, Geophys. Res. Lett., 43, 413–421, https://doi.org/10.1002/2015GL067265, 2016.

Bowman, D., Williamson, G., Yebra, M., Lizundia-Loiola, J., Pettinari, M. L., Shah, S., Bradstock, R., and Chuvieco, E.: Wildfires: Australia needs national monitoring agency, Nature, 584, 188–191, https://doi.org/10.1038/d41586-020-02306-4, 2020.

Bowman, D. M. J. S., Balch, J., Artaxo, P., Bond, W. J., Cochrane, M. A., D'Antonio, C. M., DeFries, R., Johnston, F. H., Keeley, J. E., Krawchuk, M. A., Kull, C. A., Mack, M., Moritz, M. A., Pyne, S., Roos, C. I., Scott, A. C., Sodhi, N. S., and Swetnam, T. W.: The human dimension of fire regimes on Earth: The human dimension of fire regimes on Earth, J. Biogeogr., 38, 2223–2236, https://doi.org/10.1111/j.1365-2699.2011.02595.x, 2011.

Brull, J.: Análisis de la severidad de los incendios de magnitud de la temporada de incendios forestales 2017–2018, Sección de análisis y predicción de incendios forestales. Corporación Nacional Forestal, Santiago, Chile, pp. 67, 2018.

Butsic, V., Kelly, M., and Moritz, M.: Land Use and Wildfire: A Review of Local Interactions and Teleconnections, Land, 4, 140–156, https://doi.org/10.3390/land4010140, 2015.

Cardil, A., Mola-Yudego, B., Blázquez-Casado, Á., and González-Olabarria, J. R.: Fire and burn severity assessment: Calibration of Relative Differenced Normalized Burn Ratio (RdNBR) with field data, J. Environ. Manage., 235, 342–349, https://doi.org/10.1016/j.jenvman.2019.01.077, 2019.

Chuvieco, E., Lizundia-Loiola, J., Pettinari, M. L., Ramo, R., Padilla, M., Tansey, K., Mouillot, F., Laurent, P., Storm, T., Heil, A., and Plummer, S.: Generation and analysis of a new global burned area product based on MODIS 250 m reflectance bands and thermal anomalies, Earth Syst. Sci. Data, 10, 2015–2031, https://doi.org/10.5194/essd-10-2015-2018, 2018.

Chuvieco, E., Mouillot, F., van der Werf, G. R., San Miguel, J., Tanase, M., Koutsias, N., García, M., Yebra, M., Padilla, M., Gitas, I., Heil, A., Hawbaker, T. J., and Giglio, L.: Historical background and current developments for mapping burned area from satellite Earth observation, Remote Sens. Environ., 225, 45–64, https://doi.org/10.1016/j.rse.2019.02.013, 2019.

de la Barrera, F., Barraza, F., Favier, P., Ruiz, V., and Quense, J.: Megafires in Chile 2017: Monitoring multiscale environmental impacts of burned ecosystems, Sci. Total Environ., 637–638, 1526–1536, https://doi.org/10.1016/j.scitotenv.2018.05.119, 2018.

Duane, A., Castellnou, M., and Brotons, L.: Towards a comprehensive look at global drivers of novel extreme wildfire events, Clim. Change, 165, 43, https://doi.org/10.1007/s10584-021-03066-4, 2021.

Fassnacht, F. E., Schmidt-Riese, E., Kattenborn, T., and Hernández, J.: Explaining Sentinel 2-based dNBR and RdNBR variability with reference data from the bird's eye (UAS) perspective, Int. J. Appl. Earth Obs. Geoinf., 95, 102262, https://doi.org/10.1016/j.jag.2020.102262, 2021.

Fusco, E. J., Abatzoglou, J. T., Balch, J. K., Finn, J. T., and Bradley, B. A.: Quantifying the human influence on fire ignition across the western USA, Ecol. Appl., 26, 2390–2401, https://doi.org/10.1002/eap.1395, 2016.

Ganteaume, A. and Syphard, A. D.: Ignition Sources, in: Encyclopedia of Wildfires and Wildland-Urban Interface (WUI) Fires, edited by: Manzello, S. L., Springer International Publishing, Cham, 1–17, https://doi.org/10.1007/978-3-319-51727-8_43-1, 2018.

Garreaud, R. D., Boisier, J. P., Rondanelli, R., Montecinos, A., Sepúlveda, H. H., and Veloso-Aguila, D.: The Central Chile Mega Drought (2010–2018): A climate dynamics perspective, Int. J. Climatol., 40, 421–439, https://doi.org/10.1002/joc.6219, 2019.

Ghermandi, L., Lanorte, A., Oddi, F. J., and Lasaponara, R.: Assessing Fire Severity in Semiarid Environments with the DNBR and RDNBR Indices, Glob. J. Sci. Front. Res. H Environ. Earth Sci., 19, 27–44, 2019.

Giglio, L., Randerson, J. T., and van der Werf, G. R.: Analysis of daily, monthly, and annual burned area using the fourth-generation global fire emissions database (GFED4): ANALYSIS OF BURNED AREA, J. Geophys. Res.-Biogeo., 118, 317–328, https://doi.org/10.1002/jgrg.20042, 2013.

Giglio, L., Schroeder, W., and Justice, C. O.: The collection 6 MODIS active fire detection algorithm and fire products, Remote Sens. Environ., 178, 31–41, https://doi.org/10.1016/j.rse.2016.02.054, 2016.

Giglio, L., Boschetti, L., Roy, D. P., Humber, M. L., and Justice, C. O.: The Collection 6 MODIS burned area mapping algorithm and product, Remote Sens. Environ., 217, 72–85, https://doi.org/10.1016/j.rse.2018.08.005, 2018.

Gómez-González, S., González, M. E., Paula, S., Díaz-Hormazábal, I., Lara, A., and Delgado-Baquerizo, M.: Temperature and agriculture are largely associated with fire activity in Central Chile across different temporal periods, Forest Ecol. Manage., 433, 535–543, https://doi.org/10.1016/j.foreco.2018.11.041, 2019.

González, M. E., Gómez-González, S., Lara, A., Garreaud, R., and Díaz-Hormazábal, I.: The 2010-2015 Megadrought and its influence on the fire regime in central and south-central Chile, Ecosphere, 9, e02300, https://doi.org/10.1002/ecs2.2300, 2018.

Goodwin, N. R. and Collett, L. J.: Development of an automated method for mapping fire history captured in Landsat TM and ETM+ time series across Queensland, Australia, Remote Sens. Environ., 148, 206–221, https://doi.org/10.1016/j.rse.2014.03.021, 2014.

Gorelick, N., Hancher, M., Dixon, M., Ilyushchenko, S., Thau, D., and Moore, R.: Google Earth Engine: Planetary-scale geospatial analysis for everyone, Remote Sens. Environ., 202, 18–27, https://doi.org/10.1016/j.rse.2017.06.031, 2017.

Hawbaker, T. J., Vanderhoof, M. K., Beal, Y.-J., Takacs, J. D., Schmidt, G. L., Falgout, J. T., Williams, B., Fairaux, N. M., Caldwell, M. K., Picotte, J. J., Howard, S. M., Stitt, S., and Dwyer, J. L.: Mapping burned areas using dense time-series of Landsat data, Remote Sens. Environ., 198, 504–522, https://doi.org/10.1016/j.rse.2017.06.027, 2017.

Helman, D.: Land surface phenology: What do we really "see" from space?, Sci. Total Environ., 618, 665–673, https://doi.org/10.1016/j.scitotenv.2017.07.237, 2018.

Holz, A., Paritsis, J., Mundo, I. A., Veblen, T. T., Kitzberger, T., Williamson, G. J., Aráoz, E., Bustos-Schindler, C., González, M. E., Grau, H. R., and Quezada, J. M.: Southern Annular Mode drives multicentury wildfire activity in southern South America, P. Natl. Acad. Sci. USA, 114, 9552–9557, https://doi.org/10.1073/pnas.1705168114, 2017.

Hu, X., Ban, Y., and Nascetti, A.: Uni-Temporal Multispectral Imagery for Burned Area Mapping with Deep Learning, Remote Sens., 13, 1509, https://doi.org/10.3390/rs13081509, 2021.

Huang, C., Thomas, N., Goward, S. N., Masek, J. G., Zhu, Z., Townshend, J. R. G., and Vogelmann, J. E.: Automated masking of cloud and cloud shadow for forest change analysis using Landsat images, Int. J. Remote Sens., 31, 5449–5464, https://doi.org/10.1080/01431160903369642, 2010.

Jolly, W. M., Cochrane, M. A., Freeborn, P. H., Holden, Z. A., Brown, T. J., Williamson, G. J., and Bowman, D. M. J. S.: Climate-induced variations in global wildfire danger from 1979 to 2013, Nat. Commun., 6, 7537, https://doi.org/10.1038/ncomms8537, 2015.

Kelly, L. T., Giljohann, K. M., Duane, A., Aquilué, N., Archibald, S., Batllori, E., Bennett, A. F., Buckland, S. T., Canelles, Q., Clarke, M. F., Fortin, M.-J., Hermoso, V., Herrando, S., Keane, R. E., Lake, F. K., McCarthy, M. A., Morán-Ordóñez, A., Parr, C. L., Pausas, J. G., Penman, T. D., Regos, A., Rumpff, L., Santos, J. L., Smith, A. L., Syphard, A. D., Tingley, M. W., and Brotons, L.: Fire and biodiversity in the Anthropocene, Science, 370, eabb0355, https://doi.org/10.1126/science.abb0355, 2020.

Key, C. H. and Benson, N. C.: The normalized burn ratio (NBR): A Landsat TM radiometric measure of burn severity. US Geological Survey Northern Rocky Mountain Science Center. U.S. Department of the Interior, U.S. Geological Survey, Northern Rocky Mountain Science Center, 2003.

King, M. D., Platnick, S., Menzel, W. P., Ackerman, S. A., and Hubanks, P. A.: Spatial and Temporal Distribution of Clouds Observed by MODIS Onboard the Terra and Aqua Satellites, IEEE Ts. Geosci. Remote, 51, 3826–3852, https://doi.org/10.1109/TGRS.2012.2227333, 2013.

Knopp, L., Wieland, M., Rättich, M., and Martinis, S.: A Deep Learning Approach for Burned Area Segmentation with Sentinel-2 Data, Remote Sens., 12, 2422, https://doi.org/10.3390/rs12152422, 2020.

Lentile, L. B., Holden, Z. A., Smith, A. M. S., Falkowski, M. J., Hudak, A. T., Morgan, P., Lewis, S. A., Gessler, P. E., and Benson, N. C.: Remote sensing techniques to assess active fire characteristics and post-fire effects, Int. J. Wildland Fire, 15, 319, https://doi.org/10.1071/WF05097, 2006.

Lizundia-Loiola, J., Franquesa, M., Boettcher, M., Kirches, G., Pettinari, M. L., and Chuvieco, E.: Implementation of the Burned Area Component of the Copernicus Climate Change Service: From MODIS to OLCI Data, Remote Sens., 13, 4295, https://doi.org/10.3390/rs13214295, 2021.

Long, T., Zhang, Z., He, G., Jiao, W., Tang, C., Wu, B., Zhang, X., Wang, G., and Yin, R.: 30 m Resolution Global Annual Burned Area Mapping Based on Landsat Images and Google Earth Engine, Remote Sens., 11, 489, https://doi.org/10.3390/rs11050489, 2019.

McWethy, D. B., Pauchard, A., García, R. A., Holz, A., González, M. E., Veblen, T. T., Stahl, J., and Currey, B.: Landscape drivers of recent fire activity (2001–2017) in south-central Chile, PLOS ONE, 13, e0201195, https://doi.org/10.1371/journal.pone.0201195, 2018.

Miller, J. D. and Thode, A. E.: Quantifying burn severity in a heterogeneous landscape with a relative version of the delta Normalized Burn Ratio (dNBR), Remote Sens. Environ., 109, 66–80, https://doi.org/10.1016/j.rse.2006.12.006, 2007.

Miranda, A., Altamirano, A., Cayuela, L., Lara, A., and González, M.: Native forest loss in the Chilean biodiversity hotspot: revealing the evidence, Reg. Environ. Change, 17, 285–297, https://doi.org/10.1007/s10113-016-1010-7, 2017.

Miranda, A., Carrasco, J., González, M., Pais, C., Lara, A., Altamirano, A., Weintraub, A., and Syphard, A. D.: Evidence-based mapping of the wildland-urban interface to better identify human communities threatened by wildfires, Environ. Res. Lett., 15, 094069, https://doi.org/10.1088/1748-9326/ab9be5, 2020.

Miranda, A., Mentler, R., Moleto-Lobos, I., Alfaro, G., Aliaga, L., Balbontín, D., Barraza, M., Baumbach, S., Calderón, P., Cárdenas, F., Castillo, I., Gonzalo, C., de la Barra, F., Galleguillos, M., González, M., Hormazábal, C., Lara, A., Mancilla, I., Muñoz, F., Oyarce, C., Pantoja, F., Ramírez, R., and Urrutia, V. Fire Scars: remotely sensed historical burned area and fire severity in Chile between 1984–2018, PANGAEA [data set], https://doi.org/10.1594/PANGAEA.941127, 2022.

Moritz, M. A., Batllori, E., Bradstock, R. A., Gill, A. M., Handmer, J., Hessburg, P. F., Leonard, J., McCaffrey, S., Odion, D. C., Schoennagel, T., and Syphard, A. D.: Learning to coexist with wildfire, Nature, 515, 58–66, https://doi.org/10.1038/nature13946, 2014.

Pettorelli, N., Vik, J. O., Mysterud, A., Gaillard, J.-M., Tucker, C. J., and Stenseth, N. Chr.: Using the satellite-derived NDVI to assess ecological responses to environmental change, Trends Ecol. Evol., 20, 503–510, https://doi.org/10.1016/j.tree.2005.05.011, 2005.

Pinto, M. M., Trigo, R. M., Trigo, I. F., and DaCamara, C. C.: A Practical Method for High-Resolution Burned Area Monitoring Using Sentinel-2 and VIIRS, Remote Sens., 13, 1608, https://doi.org/10.3390/rs13091608, 2021.

Radeloff, V. C., Helmers, D. P., Kramer, H. A., Mockrin, M. H., Alexandre, P. M., Bar-Massada, A., Butsic, V., Hawbaker, T. J., Martinuzzi, S., Syphard, A. D., and Stewart, S. I.: Rapid growth of the US wildland-urban interface raises wildfire risk, P. Natl. Acad. Sci. USA, 115, 3314–3319, https://doi.org/10.1073/pnas.1718850115, 2018.

Ramo, R., Roteta, E., Bistinas, I., van Wees, D., Bastarrika, A., Chuvieco, E., and van der Werf, G. R.: African burned area and fire carbon emissions are strongly impacted by small fires undetected by coarse resolution satellite data, P. Natl. Acad. Sci. USA, 118, e2011160118, https://doi.org/10.1073/pnas.2011160118, 2021.

Roteta, E., Bastarrika, A., Padilla, M., Storm, T., and Chuvieco, E.: Development of a Sentinel-2 burned area algorithm: Generation of a small fire database for sub-Saharan Africa, Remote Sens. Environ., 222, 1–17, https://doi.org/10.1016/j.rse.2018.12.011, 2019.

Rouse, J. W., Haas, R. H., Schell, J. A., and Deering, D. W.: Monitoring vegetation systems in the Great Plains with ERTS, in: Third Earth Resources Technology Satellite–1 Syposium, edited by: Freden, S. C., Mercanti, E. P., and Becker, M., Volume I: Technical Presentations, NASA SP-351, NASA, Washington, D.C., 309–317, 1974.

Roy, D. P., Ju, J., Mbow, C., Frost, P., and Loveland, T.: Accessing free Landsat data via the Internet: Africa's challenge, Remote Sens. Lett., 1, 111–117, https://doi.org/10.1080/01431160903486693, 2010.

Schroeder, W., Oliva, P., Giglio, L., and Csiszar, I. A.: The New VIIRS 375m active fire detection data product: Algorithm description and initial assessment, Remote Sens. Environ., 143, 85–96, https://doi.org/10.1016/j.rse.2013.12.008, 2014.

Singh, M., Evans, D., Tan, B. S., and Nin, C. S.: Mapping and Characterizing Selected Canopy Tree Species at the Angkor World Heritage Site in Cambodia Using Aerial Data, PLOS ONE, 10, e0121558, https://doi.org/10.1371/journal.pone.0121558, 2015.

Soulard, C., Albano, C., Villarreal, M., and Walker, J.: Continuous 1985–2012 Landsat Monitoring to Assess Fire Effects on Meadows in Yosemite National Park, California, Remote Sens., 8, 371, https://doi.org/10.3390/rs8050371, 2016.

Soverel, N. O., Perrakis, D. D. B., and Coops, N. C.: Estimating burn severity from Landsat dNBR and RdNBR indices across western Canada, Remote Sens. Environ., 114, 1896–1909, https://doi.org/10.1016/j.rse.2010.03.013, 2010.

Stenzel, J. E., Bartowitz, K. J., Hartman, M. D., Lutz, J. A., Kolden, C. A., Smith, A. M. S., Law, B. E., Swanson, M. E., Larson, A. J., Parton, W. J., and Hudiburg, T. W.: Fixing a snag in carbon emissions estimates from wildfires, Glob. Change Biol., 25, 3985–3994, https://doi.org/10.1111/gcb.14716, 2019.

Stillinger, T., Roberts, D. A., Collar, N. M., and Dozier, J.: Cloud Masking for Landsat 8 and MODIS Terra Over Snow-Covered Terrain: Error Analysis and Spectral Similarity Between Snow and Cloud, Water Resour. Res., 55, 6169–6184, https://doi.org/10.1029/2019WR024932, 2019.

Stougiannidou, D., Zafeiriou, E., and Raftoyannis, Y.: Forest Fires in Greece and Their Economic Impacts on Agriculture, KnE Soc. Sci., 54–70, https://doi.org/10.18502/kss.v4i1.5977, 2020.

Szpakowski, D. M. and Jensen, J. L. R.: A Review of the Applications of Remote Sensing in Fire Ecology, Remote Sens., 11, 2638, https://doi.org/10.3390/rs11222638, 2019.

Úbeda, X. and Sarricolea, P.: Wildfires in Chile: A review, Global Planet. Change, 146, 152–161, https://doi.org/10.1016/j.gloplacha.2016.10.004, 2016.

Urrutia-Jalabert, R., González, M. E., González-Reyes, Á., Lara, A., and Garreaud, R.: Climate variability and forest fires in central and south-central Chile, Ecosphere, 9, e02171, https://doi.org/10.1002/ecs2.2171, 2018.

Viale, M., Bianchi, E., Cara, L., Ruiz, L. E., Villalba, R., Pitte, P., Masiokas, M., Rivera, J., and Zalazar, L.: Contrasting Climates at Both Sides of the Andes in Argentina and Chile, Front. Environ. Sci., 7, 69, https://doi.org/10.3389/fenvs.2019.00069, 2019.

van Wagtendonk, J. W., Root, R. R., and Key, C. H.: Comparison of AVIRIS and Landsat ETM+ detection capabilities for burn severity, Remote Sens. Environ., 92, 397–408, https://doi.org/10.1016/j.rse.2003.12.015, 2004.

Wulder, M. A., White, J. C., Loveland, T. R., Woodcock, C. E., Belward, A. S., Cohen, W. B., Fosnight, E. A., Shaw, J., Masek, J. G., and Roy, D. P.: The global Landsat archive: Status, consolidation, and direction, Remote Sens. Environ., 185, 271–283, https://doi.org/10.1016/j.rse.2015.11.032, 2016.